# Supporting Information

Rao et al. 10.1073/pnas.1316453111

## SI Materials and Methods

**Cloning, Expression, and Purification of the Est3 Protein.** The *Saccharomyces cerevisiae* Est3 gene was cloned into a pET–$His_{10}$–Smt3 (Smt3 is yeast SUMO) expression vector (1). The final Est3 mutant construct (referred to as "$Est3^{\Delta N}$" in the text) contains a deletion of the first 12 residues plus the Cys142Ser mutation and was made by side-directed mutagenesis. Proteins were expressed from *Escherichia coli* BL21(DE3) cells in Luria Broth (LB) by induction with isopropyl β-D-1-thiogalactopyranoside (IPTG) and postinduction growth for 24 h at 15 °C. Cells were harvested by centrifugation and the resulting cell pellet resuspended and lysed in lysis buffer [buffer A: 100 mM potassium phosphate buffer (pH 7.5), 100 mM sodium sulfate ($Na_2SO_4$), 10% (vol/vol) glycerol, 10 mM imidazole and 3 mM βME, and an EDTA-free protease inhibitor mixture tablet (Roche)]. Postlysis supernatant was subjected to $Ni^{2+}$-affinity chromatography by gravity flow (GE Healthcare) and eluted. $His_{10}$–SUMO–$Est3^{\Delta N}$ was incubated with SUMO specific protease, Ulp1, to cleave off the $His_{10}$–SUMO tag (1) and further purified by size-exclusion chromatography (Superdex75, GE Healthcare) in buffer B [100 mM potassium phosphate buffer (pH 7.5), 100 mM $Na_2SO_4$, 5% (vol/vol) glycerol, and 3 mM βME]. A second round of $Ni^{2+}$-affinity chromatography (in buffer B) led to separation of untagged $Est3^{\Delta N}$ from the contaminating $His_{10}$–SUMO tag. $Est3^{\Delta N}$ eluted at >95% purity and was concentrated and buffer exchanged to the experimentally appropriate buffer, using a 9000 MWCO protein concentrator (Pierce).

$^{15}N$-labeled $Est3^{\Delta N}$ protein was expressed in *E. coli* BL21 (DE3) in minimal M9 growth medium (2), supplemented with 1× MEM vitamin solution (Invitrogen), 1× Metal Mix (2), and 50 mg/L kanamycin; 2 g/L glucose provided the sole carbon source. For uniformly $^{15}N$,$^{13}C$-labeled $Est3^{\Delta N}$, 2 g/L of [$^{13}C$] glucose (Sigma/Isotec) was used. *E. coli* BL21(DE3) pLysS cells were used for expression of uniformly $^{2}H$,$^{15}N$,$^{13}C$-labeled $Est3^{\Delta N}$ protein and labeling protocol adapted from previous description (3). In short, a culture grown in LB at 37 °C was harvested by centrifugation, resuspended in M9/$H_2O$ (3), and grown at 37 °C to an $OD_{600}$ of 0.5. Cells were harvested and resuspended in 50 mL M9/$D_2O$, supplemented with 2 g/L [$^{2}H$,$^{13}C$] glucose (Sigma/Isotec) as the sole carbon source, 1.5 g/L ammonium-$^{15}N_2$ sulfate as the sole nitrogen source, and 4% (wt/vol) $^{13}C$,$^{15}N$,D Isogro (Sigma/Isotec). At an $OD_{600}$ of 0.5, the cells were transferred to 1 L of M9/$D_2O$, grown to $OD_{600}$ of ∼0.9 and cold-shocked on ice for ∼1 h. Protein expression was induced with 1.0 mM IPTG, followed by postinduction growth for 24 h at 15 °C. The proteins were purified as described above.

Selective Ile, Leu, and Val (ILV) methyl-protonated sample was prepared as described elsewhere (4), with some modifications. The cell growth protocol was the same as for uniformly $^{2}H$,$^{15}N$,$^{13}C$-labeling $Est3^{\Delta N}$ protein until transfer to 1 L M9/$D_2O$. At an $OD_{600}$ of ∼0.9, M9/$D_2O$ was supplemented with ILV methyl-protonated precursors; 100 mg/L 2-keto-3-(methyl-$d_3$)-butyric acid-1,2,3,4-$^{13}C_4$,3-$d_1$ sodium salt and 50 mg/L 2-ketobutyic acid-$^{13}C_4$,3,3-$d_2$ sodium salt (Isotec). The M9/$D_2O$ culture was grown for another ∼1.5 h, followed by cold-shock on ice for ∼1 h, induction of protein expression with 1.0 mM IPTG, and postinduction growth for ∼30 h at 15 °C. The protein was purified as described above.

**High-Throughput Screening for NMR Sample Buffer for Est3.** A high-throughput microdrop screening strategy was used to arrive at NMR buffer components for the $Est3^{\Delta N}$ protein (initially stored in buffer B). The screens were set up and scored as described elsewhere (5), with some modifications. Initial screening trays were set up on Intelli-Plate 96-well plates on an Art Robbins Instruments Crystal Phoenix automated drop-setter. Lindwall Screen (6) and preformulated 96-well ready buffers from Hampton Research [Detergent Screen HT(HR2-406), Additive Screen HT (HR2-138), Additive Screen (HR2-428), SaltRx HT(HR2-136)] were tested for enhancing $Est3^{\Delta N}$ solubility. Identified conditions were confirmed manually by setting drops in a 24-well tray. Finally, a manually confirmed condition was retested for solubility in a 50-μL volume. The screens identified low-conductivity buffering salts (7), Bis-Tris propane and Mops, as well as the additives arginine, glutamic acid, and the nondetergent sulfobetaine NDSB-195 as being favorable for protein stability and NMR. The NMR sample buffer (Buffer C) was 50 mM Bis-Tris propane/Mops (pH 7.1), 50 mM $Na_2SO_4$, 100 mM arginine, 100 mM glutamic acid, 100 mM NDSB-195, and 2 mM DTT.

**NMR Spectroscopy.** All NMR data were collected at 25 °C on ∼280-μM samples in buffer C. $^{2}H$,$^{13}C$,$^{15}N$-labeled $Est3^{\Delta N}$ protein was used for transverse relaxation-optimized spectroscopy (TROSY) and non–TROSY heteronuclear single-quantum coherance (HSQC) experiments and chemical shifts referenced to 2,2,3,3-$d_4$-3-(trimethylsilyl)-propionic acid. Backbone assignments were done with $^{2}H$,$^{13}C$,$^{15}N$-labeled $Est3^{\Delta N}$ sample using TROSY versions of the BioPack pulse-sequences for the following experiments: HNCA, HN(CA)CB, HN(CO)CA, HN(COCA)CB, HNCO, and $^{15}N$ NOESY-HSQC with a short mixing time (150 ms). The HNCO and $^{15}N$ NOESY-HSQC spectra were collected on an Agilent DD2 900 MHz spectrometer equipped with a salt-tolerant hydrogen cyanide (HCN) cryogenically cooled probe. All other experiments used an Agilent VNMRS 800 MHz spectrometer equipped with a salt-tolerant HCN cryogenically cooled probe. The Pine server (8) was used for automated backbone assignments followed by manual confirmation of assignments in the CcpNMR (9) analysis software. Backbone assignment was 97% complete and the chemical shifts table was deposited in the Biological Magnetic Resonance Bank.

In addition to backbone assignments, distance and orientational restraints were obtained for structure calculation. Assignment of $^{15}N$ NOESY-HSQC, on the $^{2}H$,$^{13}C$,$^{15}N$-$Est3^{\Delta N}$ sample, with a mixing time of 250 ms produced long-distance amide $^{1}H$-$^{1}H$ NOE restraints. Assignment of 100% of ILV methyl resonances, on a selectively methyl-protonated $Est3^{\Delta N}$ sample, in a 2D $^{1}H$,$^{13}C$-HMQC spectrum used the 3D HMCMCBCA and HMCMCGCBCA spectra (10). A 3D methyl $^{1}H$-$^{1}H$ $^{13}C$ HMQC-NOESY spectrum, collected with a 450-ms mixing time, provided methyl $^{1}H$-$^{1}H$ NOE distances. In total, amide $^{1}H$-$^{1}H$ NOEs and methyl $^{1}H$-$^{1}H$ NOEs contributed 128 long-distance restraints.

Amide $^{1}H$-$^{15}N$ residual dipolar couplings (RDCs) were measured using 140 μM $^{15}N$-labeled $Est3^{\Delta N}$ in buffer C with no Pf1 phage and in ∼9.6 mg/mL liquid crystalline Pf1 phage (11). $^{15}N$-HSQC and $^{15}N$-TROSY HSQC spectra were recorded for both isotropic and aligned samples. The shift difference between the $^{15}N$ chemical shifts for HSQC versus the TROSY-HSQC spectra were calculated for the isotropic sample and then multiplied by 2 to yield the scalar coupling constant ($J$) in Hz. The RDC values ($D$) for 112 NH bond vectors were calculated by subtracting this value for $J$ from the scaled shift differences obtained from the aligned spectra (11).

Qualitative H/D exchange data for structure validation was acquired as follows. A reference $^{15}$N-HSQC spectrum was collected on protonated $^{15}$N-labeled Est3$^{\Delta N}$ sample in NMR buffer C. This sample was subsequently buffer exchanged to NMR buffer C made in $D_2O$ and $^{15}$N-HSQC spectra obtained at 7 h, 24 h, 3 d, 6 d, and 9 d after deuterated buffer exchange. The $^{15}$N-{$^1$H}–heteronuclear NOE experiments for backbone dynamics involved acquisition of a reference $^{15}$N-HSQC spectrum and an amide proton-saturated $^{15}$N-{$^1$H}–heteronuclear NOE HSQC spectrum. The values were calculated by taking the ratio of the peak heights of the nonsaturated spectrum to the peak heights of the saturated spectrum (12).

All NMR data were processed in NMRPipe (13) and spectra were analyzed with CcpNMR analysis software (9).

**Structure Calculations.** Structures were generated using resolution-adapted structural recombination (RASREC) Rosetta (14). Rosetta parameters were selected initially using a beta version of the CS-Rosetta Toolkit (15) (www.csrosetta.org), and subsequently confirmed on release of Version 1.3 of the toolkit with Rosetta 3.4 (www.rosettacommons.org) compiled with message passing interface (MPI) support. Rosetta calculations used the JANUS Supercomputer (University of Colorado Boulder) that consists of 1,368 compute nodes, each with two hexcore 2.8 GHz Intel Westmere central processing units (CPUs), 24 GB RAM, and an 800 TB Lustre filesystem. Calculations were run across 44 nodes, totaling 528 CPUs. Each calculation took 6–9 h to generate 500 RASREC-selected structures. Input parameters for the calculations were generated using TALOS+ (torsion angle likelihood obtained from shift) (16), CYANA, and in-house scripts. The 20 best-scored structures from the Rosetta output were extracted, converted to Protein Data Bank (PDB) format, and parsed for input to Xplor-NIH (17) using in-house scripts.

Xplor-NIH calculations were performed using a MacBook Pro 2.53 GHz Intel Core 2 Duo (Apple) with 4 GB RAM. All input parameters for the Rosetta calculations were converted to Xplor format using in-house scripts. Validations were performed using Xplor-NIH (17) without further refinement of the structure. This method was used to obtain statistical representations of the restraint violations. CYANA-2.1 (18) calculations were performed using a MacBook Pro 2.53 GHz Intel Core 2 Duo with 4 GB RAM. Restraints for CYANA structure calculations were obtained directly from CcpNMR Analysis (9) software and TALOS+ (16). Manually assigned NOE restraint lists were used for CYANA calculations. Structure geometry was assessed by PROCHECK (19).

**In Vivo Assessment of Telomere Function.** Effects of missense mutations in *EST3* were assessed by two assays, which measured (*i*) the ability to complement an *est3*-Δ strain in a standard loss-of-function (LOF) assay and (*ii*) the ability to disrupt telomere replication when over-expressed in the presence of the wild-type *EST3* gene [overexpression dominant negative (ODN)]. This latter assay used a yeast strain which was sensitized to defects in telomerase (due to a mutation in *YKU80*), thereby permitting rapid initial detection of *est3*$^-$ defects as an immediate reduction in viability (20–22). Missense mutations that exhibited an ODN phenotype in this viability assay were subsequently shown to have ODN effects on telomere length, as well telomere length defects in the LOF assay.


1. Mossessova E, Lima CD (2000) Ulp1-SUMO crystal structure and genetic analysis reveal conserved interactions and a regulatory element essential for cell growth in yeast. *Mol Cell* 5(5):865–876.
2. Croy JE, Fast JL, Grimm NE, Wuttke DS (2008) Deciphering the mechanism of thermodynamic accommodation of telomeric oligonucleotide sequences by the *Schizosaccharomyces pombe* protection of telomeres 1 (Pot1pN) protein. *Biochemistry* 47(15):4345–4358.
3. Gardner KH, Kay LE (1998) *Modern Techniques in Protein NMR*, eds Krishna NR, Berliner LJ (Plenum, New York), pp 27–74.
4. Warner LR, et al. (2011) Structure of the BamC two-domain protein obtained by Rosetta with a limited NMR data set. *J Mol Biol* 411(1):83–95.
5. Lepre CA, Moore JM (1998) Microdrop screening: A rapid method to optimize solvent conditions for NMR spectroscopy of proteins. *J Biomol NMR* 12(4):493–499.
6. Lindwall G, Chau M-F, Gardner SR, Kohlstaedt LA (2000) A sparse matrix approach to the solubilization of overexpressed proteins. *Protein Eng* 13(1):67–71.
7. Kelly AE, Ou HD, Withers R, Dötsch V (2002) Low-conductivity buffers for high-sensitivity NMR measurements. *J Am Chem Soc* 124(40):12013–12019.
8. Bahrami A, Assadi AH, Markley JL, Eghbalnia HR (2009) Probabilistic interaction network of evidence algorithm and its application to complete labeling of peak lists from protein NMR spectroscopy. *PLOS Comput Biol* 5(3):e1000307.
9. Vranken WF, et al. (2005) The CCPN data model for NMR spectroscopy: Development of a software pipeline. *Proteins* 59(4):687–696.
10. Tugarinov V, Kay LE (2003) Ile, Leu, and Val methyl assignments of the 723-residue malate synthase G using a new labeling strategy and novel NMR methods. *J Am Chem Soc* 125(45):13868–13878.
11. Hansen MR, Mueller L, Pardi A (1998) Tunable alignment of macromolecules by filamentous phage yields dipolar coupling interactions. *Nat Struct Biol* 5(12):1065–1074.
12. Renner C, Schleicher M, Moroder L, Holak TA (2002) Practical aspects of the 2D $^{15}$N-[$^1$H]-NOE experiment. *J Biomol NMR* 23(1):23–33.
13. Delaglio F, et al. (1995) NMRPipe: A multidimensional spectral processing system based on UNIX pipes. *J Biomol NMR* 6(3):277–293.
14. Lange OF, Baker D (2012) Resolution-adapted recombination of structural features significantly improves sampling in restraint-guided structure calculation. *Proteins* 80(3):884–895.
15. Lange OF, et al. (2012) Determination of solution structures of proteins up to 40 kDa using CS-Rosetta with sparse NMR data from deuterated samples. *Proc Natl Acad Sci USA* 109(27):10873–10878.
16. Shen Y, Delaglio F, Cornilescu G, Bax A (2009) TALOS+: A hybrid method for predicting protein backbone torsion angles from NMR chemical shifts. *J Biomol NMR* 44 (4):213–223.
17. Schwieters CDC, Kuszewski JJJ, Tjandra NN, Clore GMG (2003) The Xplor-NIH NMR molecular structure determination package. *J Magn Reson* 160(1):65–73.
18. Güntert P, Mumenthaler C, Wüthrich K (1997) Torsion angle dynamics for NMR structure calculation with the new program DYANA. *J Mol Biol* 273(1):283–298.
19. Laskowski RA, MacArthur MW, Moss DS, Thornton JM (1993) PROCHECK: A program to check the stereochemical quality of protein structures. *J Appl Cryst* 26:283–291.
20. Evans SK, Lundblad V (2002) The Est1 subunit of *Saccharomyces cerevisiae* telomerase makes multiple contributions to telomere length maintenance. *Genetics* 162(3): 1101–1115.
21. Lee J, Mandell EK, Tucey TM, Morris DK, Lundblad V (2008) The Est3 protein associates with yeast telomerase through an OB-fold domain. *Nat Struct Mol Biol* 15(9):990–997.
22. Lubin JW, Rao T, Mandell EK, Wuttke DS, Lundblad V (2013) Dissecting protein function: An efficient protocol for identifying separation-of-function mutations that encode structurally stable proteins. *Genetics* 193(3):715–725.

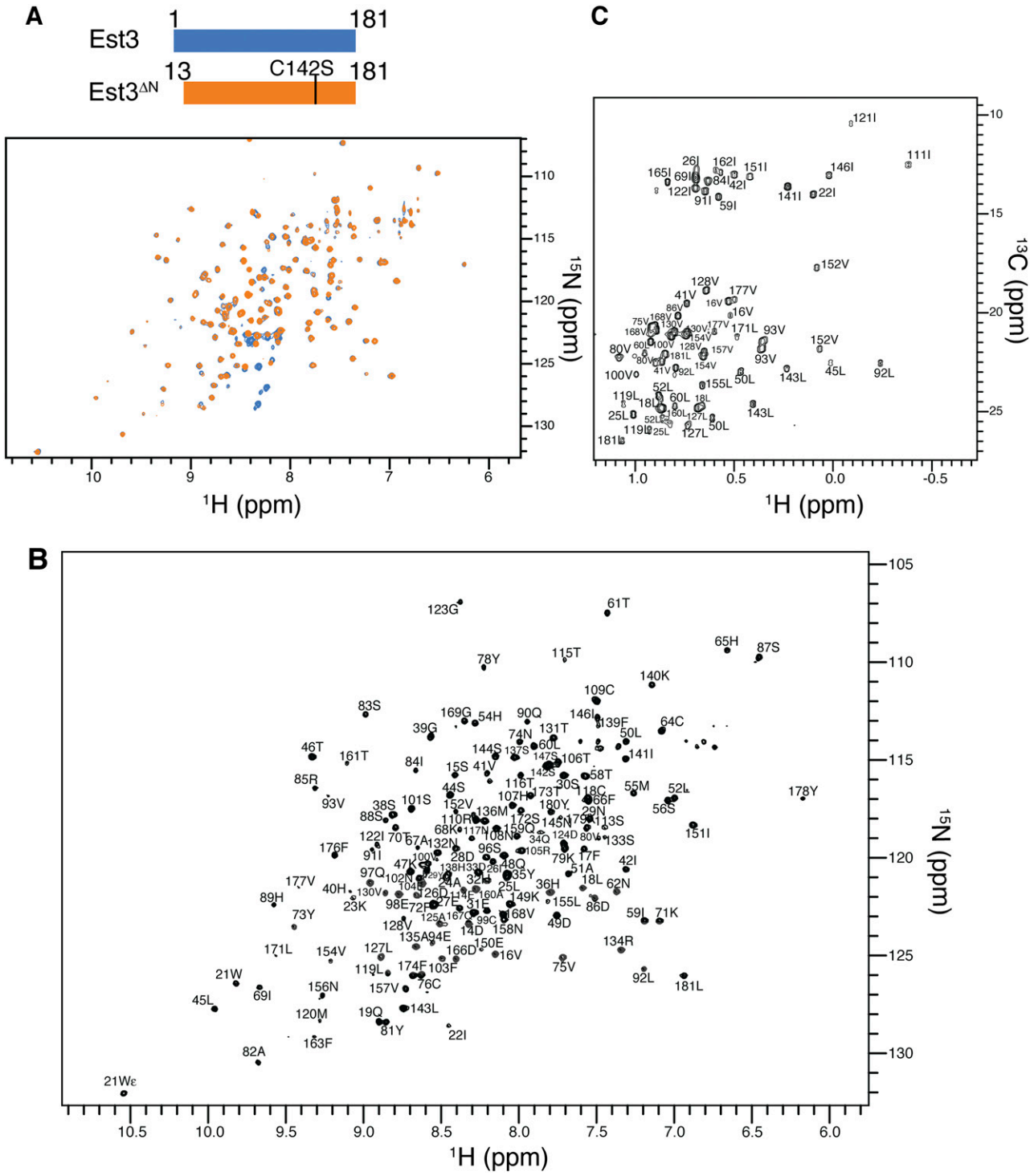


**Fig. S1.** Representative Est3$^{\Delta N}$ NMR data. (*A*) Residue boundaries are shown for the wild-type Est3 (blue) and the Est3$^{\Delta N}$ construct (orange) used for NMR experiments. $^{1}$H-$^{15}$N-HSQC spectra from wild-type Est3 (blue) and Est3$^{\Delta N}$ construct used for structure determination (orange) are superimposed. The data were collected at 800 MHz on 260 μM $^{15}$N-labeled Est3 and $^{15}$N-labeled Est3$^{\Delta N}$ in 50 mM Bis-Tris propane/Mops (pH 7.1), 50 mM $Na_2SO_4$, 100 mM arginine, 100 mM glutamic acid, 100 mM NDSB-195, and 2 mM DTT. The high intensity nonoverlapped blue peaks observed in the Est3 spectrum are due to the unstructured N-terminal tail. The close superposition of the remaining peaks shows that removal of 12 N-terminal residues and inclusion of the Cys142Ser mutation did not alter the conformation of the Est3 protein. (*B*) Assigned $^{1}$H-$^{15}$N TROSY-HSQC spectrum of Est3$^{\Delta N}$. Peaks corresponding to backbone amides are labeled with single-letter amino acid abbreviations and residue numbers. The spectrum was obtained on a 280 μM $^{2}$H,$^{13}$C,$^{15}$N-labeled Est3$^{\Delta N}$ sample at 800 MHz and 25 °C using a salt-tolerant cold probe. (*C*) Assigned $^{1}$H-$^{13}$C-HMQC spectrum of Est3$^{\Delta N}$. The peaks are labeled for methyl carbon and proton chemical shifts of the isoleucine, leucine, and valine residues (41 total). The data were collected on a 280-μM sample at 800 MHz on selectively ILV methyl-protonated $^{2}$H,$^{13}$C,$^{15}$N-labeled Est3$^{\Delta N}$ using a salt-tolerant cold probe.

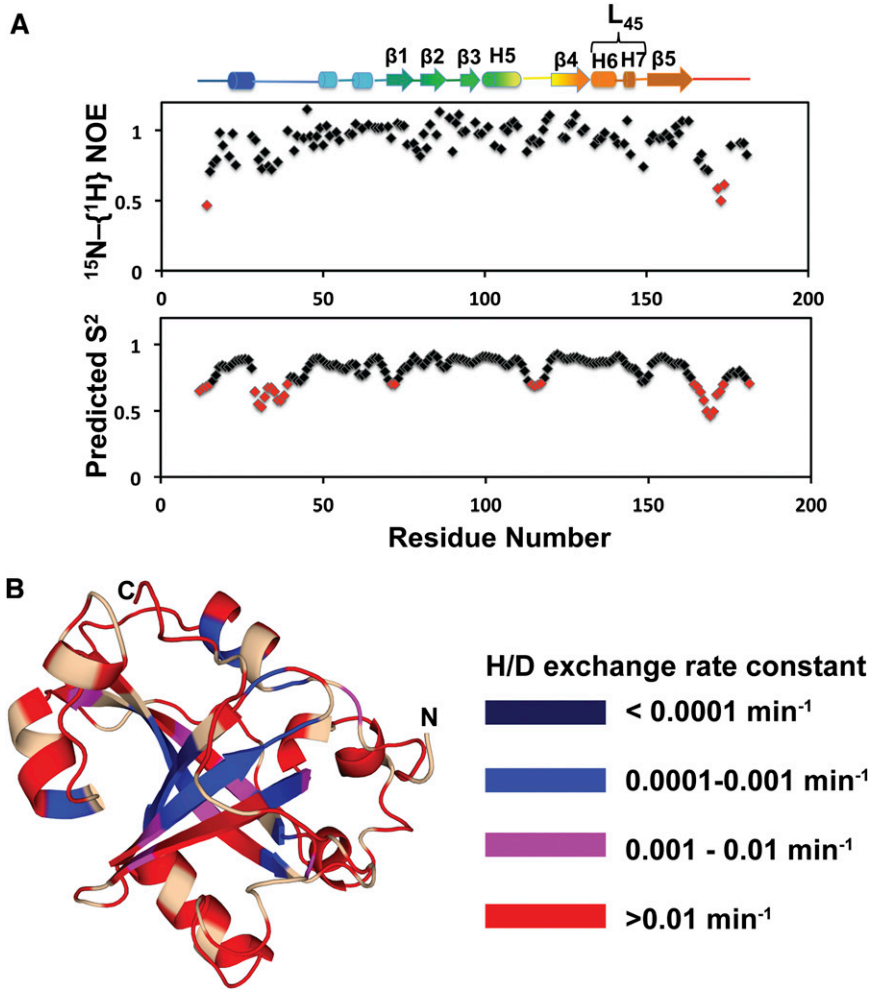


**Fig. S2.** Dynamic and H/D exchange data validate the structure. (*A*) Relaxation data show that L45 is not flexible whereas the C tail is flexible. (*Upper*) Backbone $^{15}$N-{$^{1}$H}–heteronuclear NOE values as a function of sequence. Data were collected with a 290-μM $^{15}$N-labeled Est3$^{\Delta N}$ at 800 MHz. The corresponding secondary structure elements for the residues are drawn across the top of the figure. (*Lower*) Predicted order parameter $S^2$ based on experimental chemical shifts generated by the TALOS+ server (1). (*Upper* and *Lower*) Shown in red are flexible residues of Est3 with $^{15}$N-{$^{1}$H} NOE and predicted $S^2$ values of ≤0.7. (*B*) Rates of H/D exchange for Est3 mapped on the RASREC Rosetta structure. $^{1}$H-$^{15}$N-HSQC spectra were collected at 600 MHz at 25 °C at 7, 24, 76, 141 and 215 h after exchange into 99.9% $D_2O$ buffer. Rate of exchange for residues that exchanged in the first 7 h could not be monitored, but was estimated to be >0.01 min$^{-1}$ and are colored in red. Residues that could not be monitored due to overlapped peaks and prolines are colored in wheat. Slow exchanging peaks are colored in blue and predominantly map to the β-barrel region of Est3's OB fold, confirming this region to be the protein core with low solvent accessibility.

1. Shen Y, Delaglio F, Cornilescu G, Bax A (2009) TALOS+: A hybrid method for predicting protein backbone torsion angles from NMR chemical shifts. *J Biomol NMR* 44(4):213–223.

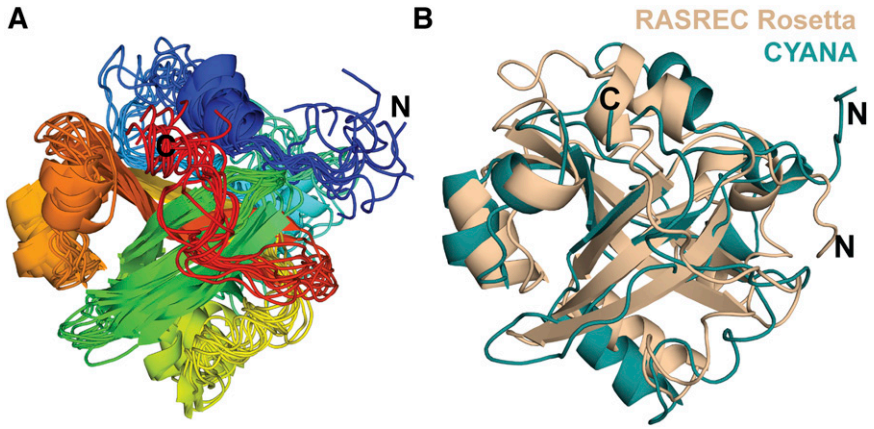


**Fig. S3.** Structure validation using traditional structure calculation. (*A*) Superposition of the lowest energy Est3$^{\Delta N}$ structures generated by CYANA-2.1 (1) using experimental restraints as an external validation for the structure generated by RASREC Rosetta using the same experimental data. (*B*) The lowest energy CYANA structure (orientation same as Fig. 1) shows similar topology to the RASREC Rosetta structure.

1. Güntert P, Mumenthaler C, Wüthrich K (1997) Torsion angle dynamics for NMR structure calculation with the new program DYANA. *J Mol Biol* 273(1):283–298.

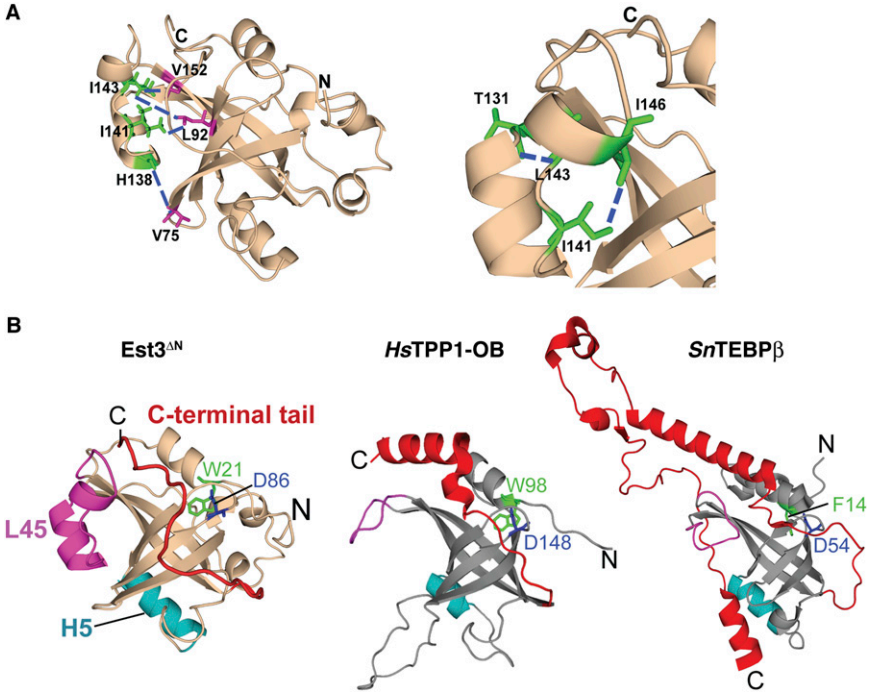


**Fig. S4.** Structure analysis and closest structural homologs of Est3 in the PDB. (*A*) Long-range NOEs define the packing of L45 against the face of the β-barrel. Four NOE connectivities (blue dashed lines) between H atoms from three residues on the L45 (colored in green) to H atoms from three residues (colored in magenta) on the β-barrel are shown: Ile143 to Val152 and Leu92; Ile141 to Leu92; and His138 to Val75. *Right* shows a magnification of L45 for two intra-L45 NOEs (*B*) *Hs*TPP1 and *Sn*TEBPβ were the top structurally similar proteins from the Dali search (1), with *Z* scores of 11.2 and 7.7, respectively. Other top Dali hits included OB-fold–containing proteins such as the DNA-binding subunit of human RPA70 (*Z* score 8.3, PDB ID code 2B3G), *Tetrahymena thermophila* TEB1 (*Z* score 7.1, PDB ID code 3U58), human RPA32 (*Z* score 7.0, PDB ID code 1QUQ), human lysyl-tRNA synthetase (*Z* score 9.0, PDB ID code 3BJU), archaeal (Sulfolobus) SSB protein (*Z* score 7.8, PDB ID code 1O7I), human Gamma-IFN–inducible protein (*Z* score 7.9, PDB ID code 2OQ0), and fission yeast Stn1 (*Z* score 6.4, PDB ID code 3KF6). Here Est3$^{\Delta N}$ (*Left*), *Hs*TPP1-OB (PDB ID code 2I46) (*Center*), and *Sn*TEBPβ (PDB ID code 2I0Q) (*Right*) are shown in the same orientation. In all structures, H5 is colored in teal, L45 is colored magenta, and the C-terminal tail is colored red. H5 is placed at an angle of ∼40° in all three structures. Trp21 (green) on helix H1 and Asp86 (blue) on loop L23 in Est3$^{\Delta N}$ corresponds to the Trp98/Asp148 pair in *Hs*TPP1 and Phe14/Asp54 pair in *Sn*TEBPβ. L45 is unusually long and structured in Est3$^{\Delta N}$, unlike L45 in *Hs*TPP1 and *Sn*TEBPβ. The C-terminal tail wraps over the β-sheet formed by strands β1, β2, and β3 in all three proteins. The C terminus ends in a helix in *Hs*TPP1-OB and bridges to the next domain of TPP1 called "POT1 binding domain" (not part of the structure). The C terminus of *Sn*TEBPβ is elaborate and structured.

1. Holm L, Rosenström P (2010) Dali server: Conservation mapping in 3D. *Nucleic Acids Res* 38(Web Server issue):W545-9.

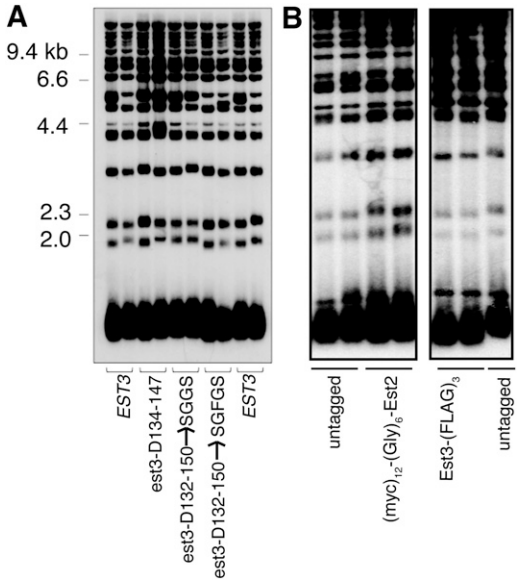


**Fig. S5.** Telomere length phenotypes of selected *est3*$^{-}$ mutations. (*A*) Telomere length of *est3*-Δ strains containing single copy plasmids expressing wild-type *EST3* or deletions or deletion/substitutions of the 19-aa L45 structured region, under the control of the native *EST3* promoter; telomere length was assessed after ~75 generations of growth. (*B*) Telomere length of strains expressing $(myc)_{12}$-$(Gly)_6$-Est2 or Est3-$(FLAG)_3$, integrated into the genome in place of the wild-type *EST2* or *EST3* loci, respectively, compared with the wild-type strain ("untagged"), also assessed after ~75 generations of growth.

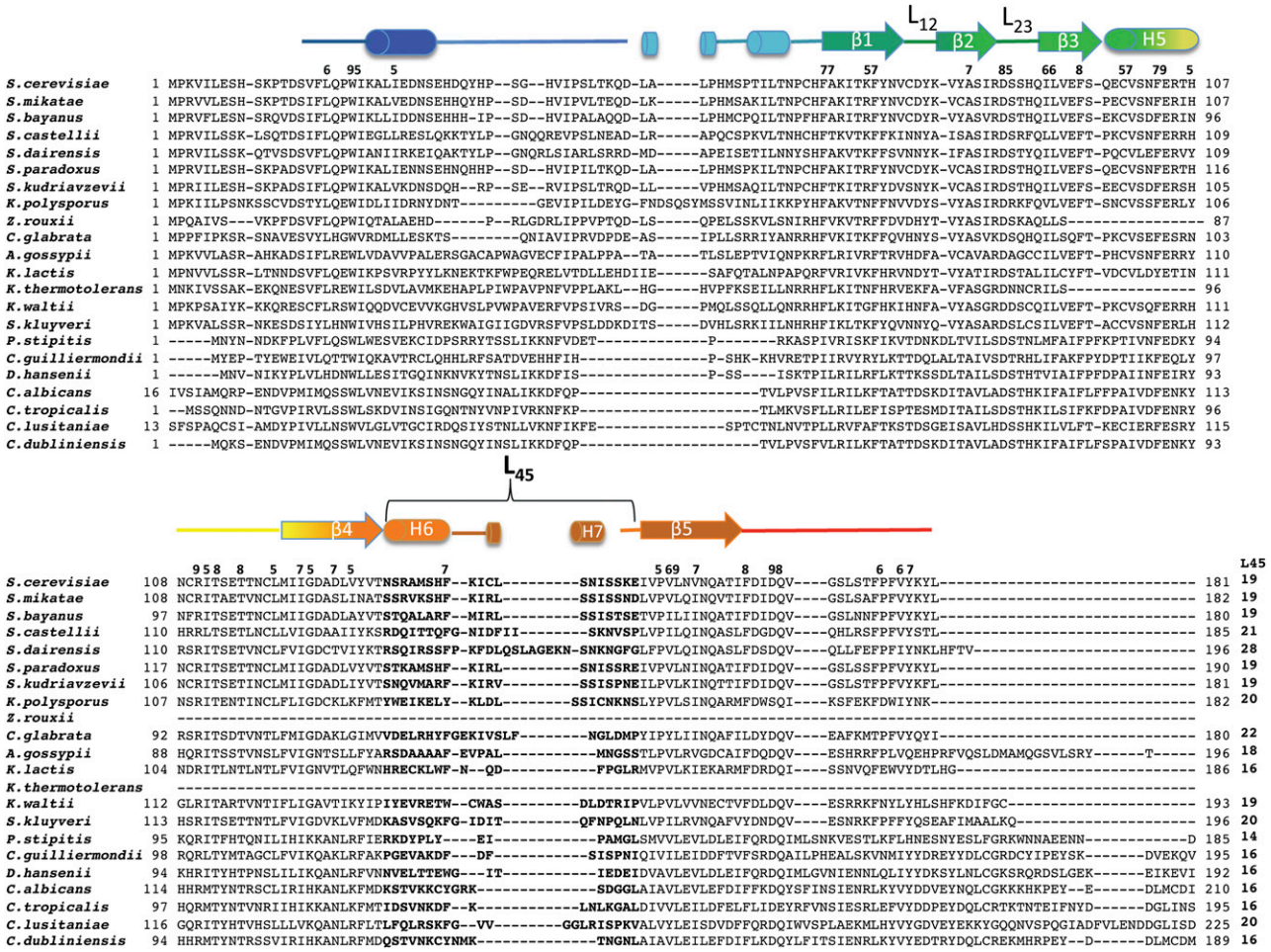


**Fig. S6.** Clustal Omega (1) alignment of Est3 proteins from 22 yeast species used for conservation mapping by ConSurf (2–4) in Fig. 4. Medium to highly conserved residues are indicated by numbers 5–9 on top of the alignment, with 9 indicating the most conserved. Secondary structure elements from RASREC Rosetta structure of Est3$^{\Delta N}$ are drawn on top of the sequence alignment. The extended loop L45 is highlighted in bold.


1. Sievers F, et al. (2011) Fast, scalable generation of high-quality protein multiple sequence alignments using Clustal Omega. *Mol Syst Biol* 7:539.
2. Ashkenazy H, Erez E, Martz E, Pupko T, Ben-Tal N (2010) ConSurf 2010: calculating evolutionary conservation in sequence and structure of proteins and nucleic acids. *Nucleic Acids Res* 38(Web Server issue):W529-33.
3. Glaser F, et al. (2003) ConSurf: Identification of functional regions in proteins by surface-mapping of phylogenetic information. *Bioinformatics* 19(1):163–164.
4. Landau M, et al. (2005) ConSurf 2005: The projection of evolutionary conservation scores of residues on protein structures. *Nucleic Acids Res* 33(Web Server issue):W299-302.

**Table S1. Structural statistics for the 20 best-scored Est3$^{\Delta N}$ RASREC Rosetta structures**

| | |
|---|---|
| No. of residues | 170 |
| NOE-based distance restraints | |
| NOE distance restraints (violations ≥0.5 Å) | 292 (64 ± 3.3) |
| Intraresidue | 0 |
| Interresidue | 292 |
| Sequential, $\|i - j\| = 1$ | 111 |
| Medium range, $\|i - j\| < 4$ | 57 |
| Long range, $\|i - j\| > 5$ | 124 |
| Other restraints | |
| φ+ψ dihedral-angle restraints (violations ≥5°)* | 254 (28 ± 3.7) |
| RDC restraints (violations ≥5 Hz) | 112 (8 ± 2.6) |
| Average RMSD to the average structure, all residues† | |
| Backbone, Å | 1.5 ± 0.16 |
| Heavy atom, Å | 2.0 ± 0.17 |
| Average RMSD to the average structure, OB fold only; residues 66–163 | |
| Backbone, Å | 0.89 ± 0.13 |
| Heavy atom, Å | 1.3 ± 0.14 |
| Ramachandran plot summary, %‡ | |
| Most favored regions | 86.0 |
| Allowed regions | 13.7 |
| Generally allowed regions | 0.3 |
| Disallowed regions | 0.0 |
| Deviations from ideal geometry | |
| Bond lengths, Å | 0.009 |
| Bond angles, ° | 0.6 |

*Torsion-angle restraints were derived from TALOS+ (1).
†RMSDs calculated using iCing server (2).
‡Analysis performed using PROCHECK (3).

1. Shen Y, Delaglio F, Cornilescu G, Bax A (2009) TALOS+: A hybrid method for predicting protein backbone torsion angles from NMR chemical shifts. *J Biomol NMR* 44(4):213-223.
2. Doreleijers JF, et al. (2012) CING: An integrated residue-based structure validation program suite. *J Biomol NMR* 54(3):267-283.
3. Laskowski RA, MacArthur MW, Moss DS, Thornton JM (1993) PROCHECK: A program to check the stereochemical quality of protein structures. *J Appl Cryst* 26:283-291.

**Table S2. Internal validation for convergence of RASREC Rosetta calculations**

| RASREC Rosetta calculation | No. of NOE constraints (% of full-set)* | Backbone RMSD to final structure† |
|---|---|---|
| Final structure | 128 (100) | |
| Validation I | 116 (90) | 1.4 |
| Validation II | 115 (90) | 1.1 |
| Validation III | 115 (90) | 0.8 |
| Validation IV | 115 (90) | 1.0 |
| Validation V | 98 (77) | 0.8 |

*Structure calculation runs were done in presence of full-set of restraints, for the final structure, and subsequent runs with depleted restraints set.
†RMSDs for backbone atoms were calculated using the "super" script in PyMOL (1).

1. Schrödinger, LLC. The PyMOL Molecular Graphics System, Version 1.5.0.4. Available at www.pymol.org.

**Table S3. List of mutations in surface-exposed Est3 residues**

| | | | |
|---|---|---|---|
| D14R | D49R | Q90R | S137E |
| S15E | L52E | E94R | H138R, H138E |
| V16E | H54R, H54E | S96E, S96R | K140E |
| F17R, F19E | M55E | Q97R | C142E |
| Q19R | S56R | E98R | S144R |
| P20E | P57R | S101R | N146R |
| K23E | T58R | N102R | I146E |
| A24R | L60E | E104R* | S148E |
| L25E | T61R | R105E | K149E |
| E27R | N62R | T106R | E150R |
| D28R | P63R | H107E, H107R | I151E |
| N29R | C64R | N108R | N156R |
| E31R | K68E* | C109R | N158R |
| H32R, H32E | T70E | R110E* | Q159R |
| D33R | K71E* | T112A, T112I** | R161R |
| Q34R | Y73R, Y73E | S113R | F163R, F163E |
| Y35R, Y35E | N74R | E114 | D164R* |
| H36E | V75E* | T116E | D166R* |
| P37E | C76R | N117K* | Q167R |
| S38R | D77R | D124R | V168E* |
| G39R | Y78R, Y78E | D126R | L171E |
| H40R, H40E | K79E | V128E | S172E |
| V41E | Y81R, Y81E | V130E | T173E |
| P43R | S83E | T131R | P175E |
| S44R | R85E | N132R | F176R, F176E |
| T46R | S87E | S133E | K179E |
| K47E | S88E | R134E | Y180R, Y180E |
| Q48R | H89E | M136E | L181E |

Surface residues were mutated by the introduction of a charged amino acid (rather than to alanine), to maximally disrupt function, and assessed for effects on telomere replication as described in Supporting Materials and Methods. Mutations with moderate to severe effects on telomere replication are highlighted in red, with more modest phenotypes indicated in pink; residues marked by an asterisk have been analyzed in previous studies (1, 2). For the three alleles that are highlighted in lavender, we have previously argued that charge-swap mutations introduced into these three residues result in partial destabilization of the mutant protein (2).

1. Lee J, Mandell EK, Tucey TM, Morris DK, Lundblad V (2008) The Est3 protein associates with yeast telomerase through an OB-fold domain. *Nat Struct Mol Biol* 15(9):990-997.
2. Lubin JW, Rao T, Mandell EK, Wuttke DS, Lundblad V (2013) Dissecting protein function: An efficient protocol for identifying separation-of-function mutations that encode structurally stable proteins. *Genetics* 193(3):715-725.